Journal of Hazardous Materials Advances 22 (2026) 101190

Contents lists available at ScienceDirect

Journal of Hazardous Materials Advances

journal homepage: www.elsevier.com/locate/hazadv

Sustainable mercury monitoring using graphitic carbon nitride as a 2D binding layer in diffusive gradient thin films

Dmitrii Deev [a,b,1], Raghuraj Singh Chouhan [b,1,*], Igor Živković [a,b], Ermira Begu [b], Ana Drinčić [c], Francisco Ruiz-Zepeda [c], Andraž Krajnc [c], Ivan Jerman [c,*], Roman Viter [d], Aleš Lapanje [b,*], Milena Horvat [b,*]

[a] Jožef Stefan International Postgraduate School, Ljubljana, Slovenia
[b] Jožef Stefan Institute, Department of Environmental Sciences, Ljubljana, Slovenia
[c] National Institute of Chemistry, Hajdrihova 19, 1000 Ljubljana, Slovenia
[d] Institute of Atomic Physics and Spectroscopy, University of Latvia, Jelgavas iela 3, Riga LV-1004, Latvia

ARTICLE INFO

Keywords:
Mercury
DGT
Graphitic carbon nitride
Adsorbent
Matrices
Non-toxic
Sustainable

ABSTRACT

Mercury (Hg) is a highly toxic and persistent environmental pollutant whose accurate monitoring remains challenging due to limitations in existing diffusive gradients in thin films (DGT) binding materials, including insufficient selectivity, complex synthesis, and sustainability concerns. In this study, we report the first application of graphitic carbon nitride (GCN) nanosheets as a metal-free and sustainable binding material for Hg^{2+} monitoring in DGT systems, addressing key limitations of current approaches. Few-layer GCN nanosheets were synthesized via thermal polymerization followed by protonation-assisted exfoliation and comprehensively characterized using X-ray diffraction (XRD), X-ray photoelectron spectroscopy (XPS), transmission electron microscopy (TEM), atomic force microscopy (AFM), Raman spectroscopy, and scanning electron microscopy (SEM).

These analyses confirmed the formation of a structurally stable, nitrogen-rich framework with abundant coordination sites. The GCN–agarose (AG–GCN) composite binding layer demonstrated high mercury binding efficiency (>90%) at environmentally relevant concentrations (2.5–10 ng/mL) and near-neutral pH, attributed to strong coordination between Hg^{2+} ions and electron-donating nitrogen sites within the heptazine structure.

Compared to conventional DGT binding phases, the proposed system offers enhanced sustainability, metal-free composition, and strong affinity toward mercury, highlighting its potential for next-generation passive environmental monitoring and advanced nanomaterial-based sensing platforms.

1. Introduction

Mercury (Hg) is one of the most hazardous global environmental pollutants due to its persistence, toxicity, and ability to bioaccumulate and biomagnify in aquatic and terrestrial ecosystems. Exposure to mercury, particularly inorganic Hg^{2+} and methylmercury species, poses severe risks to human health and ecological systems, which have led to international regulatory frameworks such as the Minamata Convention (UNEP, 2018). In aquatic environments, mercury exists in multiple chemical forms, including free ions (Hg^{2+}), chloro-complexes ($HgCl_2$ and $HgCl_4^{2-}$), and organic species, each exhibiting distinct mobility, reactivity, and bioavailability (Mason et al., 2012). Accurate monitoring of these species remains challenging due to their low environmental concentrations, complex speciation, and uncertainties in diffusion coefficients, which directly affect passive sampling approaches such as DGT that rely on Fick's law for quantification (Gade et al., 2024; Kreuzeder et al., 2015; Song et al., 2021; UNEP, 2018).

The reliability of DGT measurements critically depends on the performance of the binding layer, which must selectively and efficiently capture metal species while minimizing interference from competing ions. Conventional DGT binding materials, including Chelex-100 and polyacrylamide (APA) based systems, face several limitations. Chelex-100, based on iminodiacetate functional groups, lacks high specificity toward Hg^{2+} and is susceptible to competitive binding by abundant

* Correspondence authors.
E-mail addresses: raghuraj.chouhan@ijs.si (R.S. Chouhan), Ivan.Jerman@ki.si (I. Jerman), ales.lapanje@ijs.si (A. Lapanje), milena.horvat@ijs.si (M. Horvat).
[1] equal contribution

https://doi.org/10.1016/j.hazadv.2026.101190
Received 19 November 2025; Received in revised form 24 March 2026; Accepted 24 April 2026
Available online 25 April 2026

cations such as Fe^{3+}, Cu^{2+}, and Na^{+} in complex environmental matrices. Alternative thiol-functionalized resins and silica-based sorbents have been developed to improve selectivity (Marrugo-Madrid et al., 2024; Reichstädter et al., 2021; Zhou et al., 2018), however, these materials often involve complex synthetic routes, elevated production costs, and limited sustainability. Furthermore, some binding phases may exhibit environmental incompatibility or reduced stability under long-term deployment conditions. Some of the few examples of binding resins used in DGT applications of Hg are listed in Table 1.

These challenges highlight the need for innovative, sustainable, and cost-effective binding materials capable of strong and selective mercury coordination. GCN is a two-dimensional metal-free polymer composed of tri-s-triazine (heptazine) units, which has attracted increasing attention due to its unique structural and electronic properties. GCN possesses a high nitrogen content with abundant lone-pair electron sites capable of coordinating heavy metal ions. Previous studies have demonstrated strong interactions between GCN and mercury species, often surpassing interactions with other metal ions, indicating promising selectivity characteristics (Chouhan et al., 2023, 2021, 2019). In addition to its coordination capability, GCN offers advantages including low cost, chemical stability, environmental compatibility, tunable surface chemistry, and scalable synthesis from abundant precursors.

Despite extensive investigation of GCN in photocatalysis, sensing, and adsorption applications, (Amouzadeh Tabrizi et al., 2021; Benedet et al., 2023, 2022a, 2022b; Botelho et al., 2022; Hasija et al., 2021; Idris et al., 2020; Marchiori et al., 2025; Sreenivasulu et al., 2024), its integration as a binding phase in DGT systems has not been previously explored. The use of a nitrogen-rich, two-dimensional polymeric nanosheet as a coordination-based binding layer represents a fundamental shift from conventional functionalized resin-based systems toward intrinsic coordination-driven binding using a metal-free two-dimensional polymer. By leveraging the electron-donating nitrogen sites within the heptazine framework, it is possible to achieve strong Hg^{2+} coordination while maintaining structural stability and environmental compatibility.

Despite these advances, the use of GCN as a binding phase in DGT systems has not been previously explored, and the potential of nitrogen-rich, metal-free two-dimensional materials for passive mercury monitoring remain largely unaddressed. Existing DGT binding materials rely predominantly on functionalized resins or inorganic supports, which may involve complex preparation methods, limited sustainability, or reduced performance under environmentally relevant conditions (Marrugo-Madrid et al., 2024; Reichstädter et al., 2021; Zhou et al., 2018). Therefore, the development of a simple, scalable, and environmentally benign material with strong and selective Hg^{2+} affinity remains an important challenge.

In this study, we report the first demonstration of few-layer GCN nanosheets as a sustainable binding material for mercury monitoring in DGT systems (Scheme 1). The nanosheets were synthesized and structurally characterized using complementary techniques, including X-ray diffraction (XRD), X-ray photoelectron spectroscopy (XPS), transmission electron microscopy (TEM), atomic force microscopy (AFM), Raman spectroscopy, and scanning electron microscopy (SEM), to confirm their crystallinity, morphology, and nitrogen-rich composition. The few-layer GCN nanosheets were subsequently incorporated into an agarose matrix to fabricate a novel GCN-based DGT binding layer. The structural properties, mercury binding efficiency, and coordination mechanism were systematically investigated. To the best of our knowledge, this is the first study demonstrating few-layer GCN nanosheets as a DGT binding material for mercury, establishing a new direction for sustainable passive environmental monitoring technologies.

Table 1
List of the most recent binding resins used in DGT to capture Hg in an aqueous environment.

Binding Resin	Functionalities	Species	Reference
SiO_2-SH	sulfhydryl-modified silica cryogen	Hg(II)	(Lin et al., 2022)
3-MFS-DGT	3-mercaptopropyl silica	Hg	(Reichstädter et al., 2021)
Si(np)-TOMATS	SiO_2-NP-trioctylmethylammonium thiosalicylate	Hg(II)	(Elias et al., 2020)
TM-MDH	thiol-modified metal double hydroxide	Hg(II)	(Yao et al., 2020)
DNA-DGT	DNA-functionalized hydrogel	Hg(II)	(Pi et al., 2020)
Biomass-derived materials	biochar, canola meal, chicken feathers, cork and rice husk	labile fraction of mercury (Hg)	(Marrugo-Madrid et al., 2024)
PAN@MoS2/rGO-DGT	Polyacrylonitrile-PAN@MoS2/rGO	Hg(II)	(Lv et al., 2025)
3MFSG	3-mercaptopropyl-functionalized silica gel	Total Hg (THg)	(Noh et al., 2020)
Amberlite GT73	Thiol functionalized styrene-divinylbenzene resin	Bioavailable Hg	(Pelcová et al., 2021)
NSBA, SBA-15	aminopropyl and mercaptopropyl bi-functionalized SBA-15 nanoparticles	Hg(II)	(Yin et al., 2023)

2. Materials and methods

2.1. Chemicals and reagents

All chemicals used were of analytical grade or higher and employed without further purification. For synthesis and gel preparation, melamine monomer (99%) was used to form GCN nanosheets, and agarose (Sigma-Aldrich, USA) served as the supporting matrix. Tin(II) chloride ($SnCl_2$) solution (10% w/v) was freshly prepared by dissolving $SnCl_2{\cdot}2H_2O$ (analytical grade, Merck, Darmstadt, Germany) in 10% (v/v) hydrochloric acid (HCl). Sodium hydroxide (NaOH) solution (10 M), prepared from extra pure NaOH (Merck) in Milli-Q water, was utilized for pH adjustment during synthesis and analytical procedures.

For analytical calibration and traceability, the standard reference material (SRM) NIST 3133 mercury solution in 10% HNO_3, provided by the National Institute of Standards and Technology (NIST), was used as the primary source of Hg^{2+}. A working mercury solution (1.0498 μg/g) was prepared by titrating the diluted SRM solution with 10 M NaOH to adjust the pH to 6.5, resulting in a final ionic strength of 0.75 M. This adjustment ensured consistency with analytical conditions and improved the accuracy of mercury quantification. Traceability to NIST standards ensures reliability and comparability of mercury measurements. All glassware was rigorously cleaned by heating in a furnace at 500 °C for 5 h to eliminate potential interferences with trace-level mercury analysis.

2.2. Synthesis of GCN nanosheets

GCN was synthesized through thermal polycondensation of melamine using a procedure adapted from our previously reported optimized method (Chouhan et al., 2023). Briefly, melamine precursor was placed in a covered alumina crucible and heated in a muffle furnace under ambient atmosphere. The temperature was increased from room temperature to 550 °C at a controlled heating rate of 5 °C/min, followed by a holding time of 4 h at the final temperature to ensure complete polymerization. After the thermal treatment, the furnace was allowed to cool naturally to room temperature. The resulting yellow product was collected and ground into a fine powder to obtain bulk GCN.

This optimized thermal program was selected based on our previous study, where these conditions were found to produce well-defined layered GCN structures with improved structural uniformity. The obtained GCN powder was subsequently subjected to acid-assisted dispersion treatment to facilitate improved layer separation and

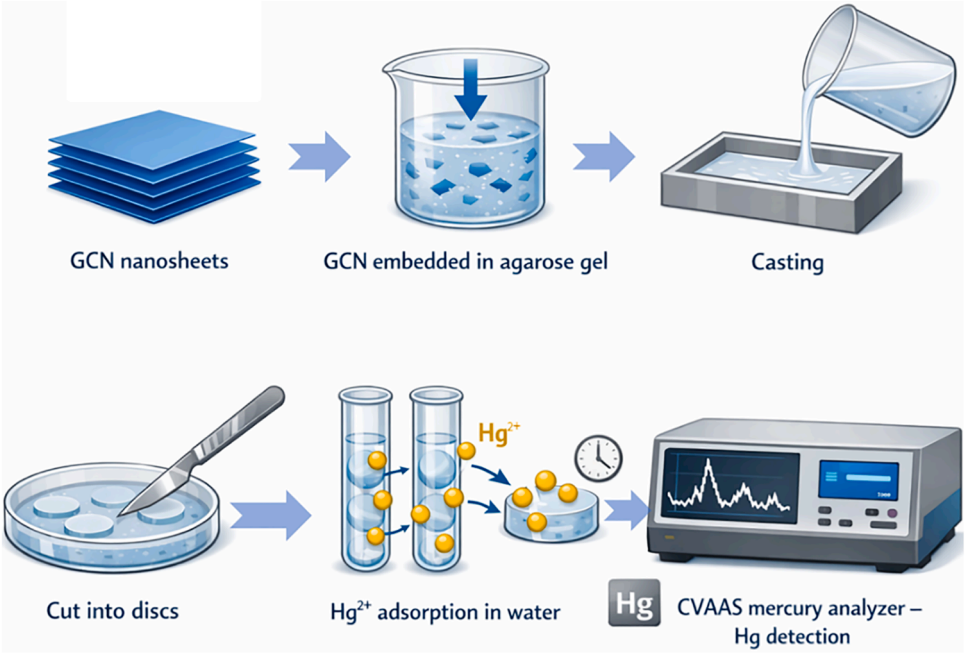

Scheme 1. Schematic representation of GCN synthesis, incorporation and binding mechanisms of Hg^{2+}.

dispersion for further characterization and adsorption experiments. To obtain a few layers of GCN nanosheets composed of a small number of stacked layers (predicted based on AFM to be 2–4 layers, see results), 3 g of the prepared powder was dispersed in 20 mL of 1 M HCl to protonate the surface and improve dispersion of the layered GCN structure and mixed for 3 h at room temperature under stirring. GCN is chemically stable and insoluble in mineral acids; therefore, the HCl treatment promotes surface protonation and dispersion rather than dissolution of the GCN framework (Chouhan et al., 2023). The solution was then filtered (0.45 μm) and dried at 70 °C. Next, 300 mg of the dried sample was dispersed in 50 mL of Mill-Q water by sonicating for 30 min, followed by centrifugation at 9000 rpm for 15 min. The supernatant was carefully decanted, and the suspension was transferred to a clean flask. Finally, after removing water by distillation or using a rotary evaporator, the product was dried overnight at 70 °C (Chouhan et al., 2023).

2.3. Characterization

The as-synthesized GCN sample was characterized using a combination of spectroscopic, microscopic, and surface characterization techniques. Fourier-transform infrared (FTIR) spectroscopy was performed on a Bruker IFS 66/S spectrometer to identify the functional groups present in the material. Powder X-ray diffraction (XRD) patterns were recorded using a high-resolution Malvern Panalytical X'Pert^3 diffractometer with CuKα$_1$ radiation (λ = 1.5407 Å) under standard measurement conditions to determine the crystalline structure. Morphological analysis was conducted using scanning electron microscopy (SEM, model unspecified) and transmission electron microscopy (TEM, JEOL), while atomic-resolution imaging was performed with scanning transmission electron microscopy (STEM, ARM 200 CF). The nanosheet thickness and height profiles were evaluated by atomic force microscopy (AFM, WITec alpha 300).

The chemical composition and elemental states were analyzed via X-ray photoelectron spectroscopy (XPS, Physical Electronics Inc., model TFA). Measurements were carried out under a chamber pressure of 6×10^{-8} Pa. The sample (200–300 mm^2) was analyzed using a monochromatic AlKα source (1486.6 eV), and photoelectrons were collected at 45° relative to the sample surface. Survey scans were acquired with a pass energy of 187.84 eV and an energy resolution of 0.5 eV. High-resolution C 1s spectra were recorded with a pass energy of 29.34 eV and a step size of 0.124 eV. Data analysis was performed using MultiPak v8.1 software (Physical Electronics, Japan), and spectra were fitted using a Gaussian–Lorentzian function after Shirley-type background subtraction.

Solid-state nuclear magnetic resonance (NMR) experiments were carried out on an Agilent Technologies 600 MHz NMR spectrometer equipped with a 3.2 mm NB double-resonance HX MAS solids probe. Cross-polarization (CP) and magic-angle spinning (MAS) techniques were applied for both ^{13}C and ^{15}N measurements, with high-power proton decoupling during acquisition. Spectra were recorded at a spinning rate of 16 kHz for ^{13}C and 10 kHz for ^{15}N. Chemical shifts were referenced to tetramethylsilane (^{13}C) and nitromethane (^{15}N).

2.4. Preparation of binding gel

Binding gels were prepared by dissolving agarose in 10 mL of Milli-Q water (resistivity 18.2 MΩ·cm) under gentle heating and continuous stirring until complete dissolution was achieved. GCN nanosheets were dispersed in Milli-Q water at an optimized concentration of 80 mg/mL and sonicated for 20 min at 37 kHz (sweep mode) using an ultrasonic bath to ensure homogeneous dispersion. The resulting GCN suspension was subsequently mixed with the hot agarose solution at a volumetric ratio of 1:5 and vortexed vigorously to obtain a uniform GCN–agarose composite (hereafter referred to as AG–GCN).

Control gels (AG) were prepared using the same procedure, except that Milli-Q water was added instead of the GCN suspension, thereby maintaining equivalent diffusion characteristics. Both AG–GCN and AG mixtures were immediately cast onto preheated, acid-cleaned glass plates (90 °C) using Teflon spacers of 0.5 mm thickness. After cooling to ambient temperature, the gels were cut into circular discs (28 mm diameter) using a sterile puncher. The AG discs served as blanks for comparative adsorption and diffusion analyses. All gel discs were stored in Milli-Q water at 4 °C until further use.

The resulting AG–GCN composite gel, consisting of GCN nanosheets homogeneously dispersed within the agarose matrix, was engineered to function as the binding layer in the DGT device. This functional layer enables the selective binding of Hg^{2+} ions following their diffusion through the diffusive gel, thereby allowing their subsequent recovery

and quantification through standard elution and analytical procedures.

2.5. GCN binding studies

To investigate the influence of surface chemistry and ionization states on the adsorption efficiency of GCN toward Hg^{2+}, a series of batch adsorption experiments were conducted by systematically varying key parameters, including solution pH, GCN dosage, initial Hg^{2+} concentration, and exposure time. The effect of pH was examined by adjusting the solution pH from 2 to 12 using dilute HCl and NaOH to identify optimal conditions for electrostatic interactions and complexation with nitrogen lone pairs on GCN. Although natural aquatic systems generally exhibit pH values between 6 and 8; extending the pH range allowed evaluation of GCN behaviour under both acidic and alkaline extremes. This approach enables determination of the material's isoelectric point and elucidation of the effects of protonation and deprotonation of surface functional groups, particularly nitrogen sites bearing lone electron pair, which are hypothesized to play a central role in Hg^{2+} coordination (Chouhan et al., 2023). Understanding pH-dependent behaviour is critical for mechanistic insight and for assessing GCN performance under environmental scenarios where pH fluctuations are common.

The influence of GCN dosage was assessed by introducing different concentrations (5–100 mg/mL) into Hg^{2+} solutions of 100 ng/mL at the optimal pH and measuring residual Hg^{2+} concentration after equilibration under mild agitation. Subsequent experiments evaluated the effect of varying Hg^{2+} concentrations (50–300 ng/mL) using the optimized GCN dosage (40 mg/mL) at near-neutral pH (6.5). The Hg^{2+} concentrations used in the study exceed typical background levels in natural water (1–100 ng/L); this elevated range was intentionally selected to ensure measurable and reproducible adsorption signals within the analytical capabilities of standard instrumentation (e.g., cold vapor atomic absorption spectrometry) without requiring pre-concentration procedures. Furthermore, these concentrations simulate conditions associated with localized contamination events, such as mercury spills or industrial effluent discharges, where pollutant levels can substantially exceed environmental baselines. Thus, the chosen concentration range remains environmentally relevant for applications in high-risk or contaminated sites. Finally, adsorption studies were conducted by maintaining a fixed Hg^{2+} concentration (100 ng/mL) while varying the contact time from 20 to 100 min. In all experiments, the residual Hg^{2+} was measured, and the adsorption efficiency was calculated accordingly. All studies were conducted at ambient temperature (25 ± 1 °C) and in triplicate to ensure reproducibility and statistical reliability.

2.6. Testing and analysis of AG-GCN mercury binding efficiency

The performance of the AG-GCN binding gels was evaluated in aqueous solutions. Gel samples were immersed in 20 mL of Milli-Q water spiked with Hg^{2+} at concentrations of 2.5, 5, and 10 ng/mL. These concentrations were selected to represent environmentally relevant levels typically found in freshwater systems affected by industrial or mining activities (Eckley et al., 2023), to correspond with the binding capacity of the GCN-based materials, and to align with regulatory thresholds, such as the U.S. EPA maximum contaminant level of 2 ng/mL.

Three sample types were examined to assess mercury-binding performance: (i) AG-GCN gels containing embedded few-layer GCN sheets, (ii) bare GCN powder suspended in Milli-Q water at a concentration equivalent to that present in AG-GCN gels, and (iii) agarose-only gels (AG) without GCN, serving as controls. Blank samples of AG-GCN and AG gels in Milli-Q water without mercury were also prepared to determine baseline signals.To account for the potential reduction of Hg^{2+} during prolonged incubation, a stability control was prepared by spiking the appropriate amount of NIST 3133 standard into 20 mL of Milli-Q water without any gels. The pH of all solutions was adjusted to 6.5 using 10 M NaOH. The samples were then tightly capped and sealed in zip-lock plastic bags followed by incubation at room temperature for 24 h. After incubation, gel samples were leached with 10 mL of 6 M HNO_3 for 24 h to extract bound mercury. The GCN-depleted supernatant was diluted with MQ water and analyzed for Hg content using cold vapour atomic absorption spectrometry (CVAAS) on a Hg-201 mercury analyzer (Sanso Seisakusho Co. Ltd., Tokyo, Japan). The fraction of unbound mercury was directly determined from the water phase.

2.7. Analytical methods for mercury quantification

The Hg^{2+} concentrations in aqueous solutions and gel matrices were determined using cold vapor atomic absorption spectrometry (CVAAS; Hg-201 Mercury Analyzer, Sanso Seisakusho Co. Ltd., Tokyo, Japan). Calibration was performed using a certified mercury standard (NIST SRM 3133) to ensure traceability and comparability of results.

After 24 h exposure to Hg^{2+}-spiked solutions (2.5, 5, and 10 ng/mL), the samples were subjected to leaching with 10 mL of 6 M HNO_3 to extract adsorbed mercury (Rodríguez Martín-Doimeadios et al., 2003; Rodríguez Martín-Doimeadios et al., 2004). Gel-bound Hg^{2+} in AG-GCN discs was recovered via overnight digestion in concentrated HNO_3 under controlled conditions. Aliquots containing approximately 1 ng Hg were transferred to a reaction vessel and reduced to elemental mercury (Hg^0) using a freshly prepared 10% $SnCl_2$ solution in 10% HCl. The system was aerated until equilibrium was reached, allowing Hg^0 vapor to be transported into the absorption cell via a four-way valve. Acidic gases were removed using an inline acid-gas trap containing 10% NaOH solution.

The amount of Hg^{2+} in the aqueous phase was calculated by comparing the peak height with that of the corresponding Hg^{2+} standard. Residual Hg^{2+} concentrations in solution and total recovered mercury from the gels were used to assess adsorption efficiency and binding performance. All measurements were conducted in triplicate under controlled laboratory conditions to ensure statistical reliability.

3. Results and discussion

3.1. Synthesis and chemical properties of GCN

The as-synthesized few-layer GCN nanosheets were systematically characterized to elucidate their structural, chemical, and morphological features. The XRD pattern shows the characteristic peaks of GCN at approximately 13.1° and 27.4°, corresponding to the (100) and (002) planes. Compared with conventional bulk GCN, the (002) peak exhibits slight broadening and reduced intensity, suggesting decreased stacking order and partial delamination of the layered structure (Fig. 1a). This observation is consistent with the formation of a few-layered GCN nanosheet, as supported by TEM and AFM analyses (Alizadeh et al., 2019). FTIR spectroscopy (Fig. 1b) displayed broad absorption bands in the 3100 and 3400 cm^{-1} region, attributed to N–H and O–H stretching vibrations, implying the presence of residual amino functionalities on the nanosheet surface (Chouhan et al., 2023). Vibrational bands observed between 1226 and 1623 cm^{-1} were assigned to C=N and C–N stretching modes, while the sharp peak at 807 cm^{-1} confirmed the retention of tris-s-triazine ring structures, collectively verifying the molecular integrity of the exfoliated GCN (Chouhan et al., 2023). These observations suggest that the thermal exfoliation process preserved the essential structural motifs while introducing surface functional groups that may enhance chemical reactivity.

To further evaluate the structural characteristics and chemical composition of the material, Raman spectroscopy was employed to verify that the transformed GCN retained its structure. The GCN exhibited D and G bands at 1360 cm^{-1} and 1582 cm^{-1} corresponding to the A_{1g} mode of sp^3-hybridized carbon in disordered graphitic regions and the in-plane E_{2g} vibration of sp^2-hybridized carbon, indicating an overall amorphous nature (Supplementary Information (SI), Figure S1) (Chouhan et al., 2023;Yu et al., 2016). Unlike graphene, the GCN framework is more intricate, making it difficult to detect signals from the

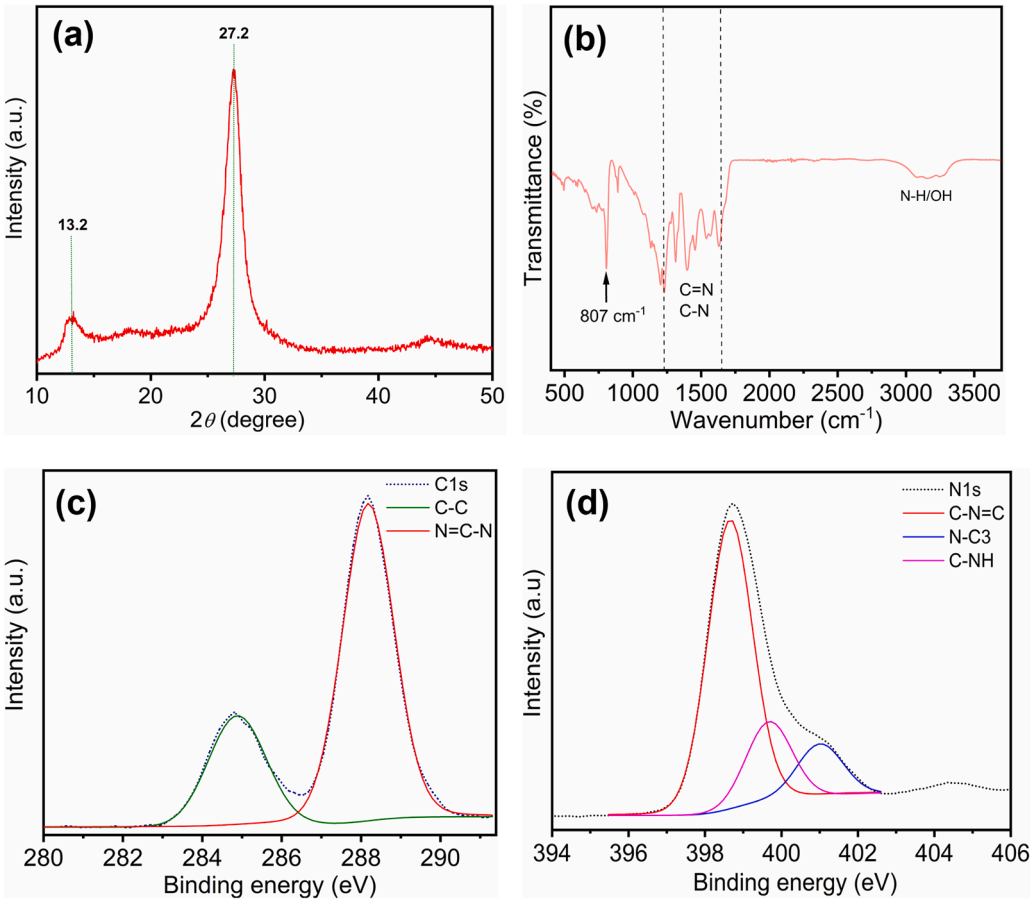

Fig. 1. Chemical characterization of GCN. (a) XRD pattern of GCN confirming its graphitic layered structure. (b) FTIR spectrum of GCN recorded in the 500–3500 cm^{-1} range, indicating characteristic amino and heterocyclic functional groups. (c) High-resolution XPS C 1s and (d) N 1s spectra, revealing distinct chemical bonding environments.

triazine units.

XPS further corroborated the chemical composition of the nanosheets (Fig. 1c, d). The C 1 s spectrum shows a dominant peak at ~284.86 eV, attributed to adventitious C-C/C=C species and a higher binding energy component ~288.15 eV corresponding to sp^2-hybridized carbon (N–C = N) within the heptazine framework (Fig. 1c)(Sun et al., 2019). The N 1s peak centred at ~398.60 eV is assigned to C=N–C species, with minor contributions at 399.90 eV (tertiary N), and 401.00 eV (C–NH or pyrrolic N), confirming the presence of amino-linked tri-s-triazine motifs (Fig. 1d) (Chouhan et al., 2019; Dyjak et al., 2015; Xu et al., 2017). The high-resolution spectra were reprocessed using the original as-acquired datasets to ensure accurate representation of peak shapes and to eliminate any truncation artefacts. Background subtraction was performed using a Shirley-type function, and peak deconvolution was carried out using Gaussian–Lorentzian functions. The subcomponents obtained by curve fitting are provided in Table S1. The quantitative elemental composition derived from the survey spectrum is summarized in Table S2. Atomic concentrations were determined from the survey spectrum using sensitivity-factor-corrected peak areas, while high-resolution spectra were used for chemical state analysis. The assignment of the fitted components is consistent with previously reported XPS studies of GCN, particularly for N–C=N, C= N–C, and C–NH environments (Chouhan et al., 2019; Dyjak et al., 2015; Xu et al., 2017).

The wide-scan High-Resolution X-ray Photoelectron Spectroscopy HRES-XPS survey spectrum recorded over the full binding energy range up to 1300 eV confirms that the material is predominantly composed of carbon and nitrogen, consistent with GCN (Figure S2). In addition, GCN survey spectra showed a high-binding-energy feature observed at ~990 eV and ~1102 eV, which correspond to the C KLL and N KLL Auger transitions, respectively, which are characteristic of nitrogen-rich carbon materials under Al Kα excitation and do not indicate the presence of extraneous elements. No other impurity-related peaks were detected (Figure S2). The high-resolution O 1s spectrum (Figure S3) exhibits a fitted component centred at 531.50 eV attributed to surface C–O, which is commonly associated with adsorbed oxygen or minor surface oxidation GCN materials. This assignment is consistent with previous reports on GCN systems (Chouhan et al., 2019; Dyjak et al., 2015; Xu et al., 2017). Overall, the combined XRD, FTIR, and XPS analyses demonstrate that the as-synthesized GCN nanosheets retain their crystallinity and molecular structure after thermal exfoliation, with surface amino groups and minor oxygen-containing species, potentially enhancing their chemical functionality. The quantitative XPS results indicate that no significant compositional changes occur during processing, confirming that the adopted treatment primarily affects structural and morphological properties rather than elemental composition.

3.2. Morphological features and elemental homogeneity of few-layer GCN nanosheets

The morphology of the synthesized few-layer GCN material was systematically characterized using SEM, TEM, and AFM. The SEM images (Fig. 2a and b) show a layered and lamellar morphology characteristic of GCN materials synthesized from melamine. Such structures typically consist of stacked sheets forming aggregated plate-like particles (Liao et al., 2018). Although SEM images provide general morphological information, they cannot definitively distinguish

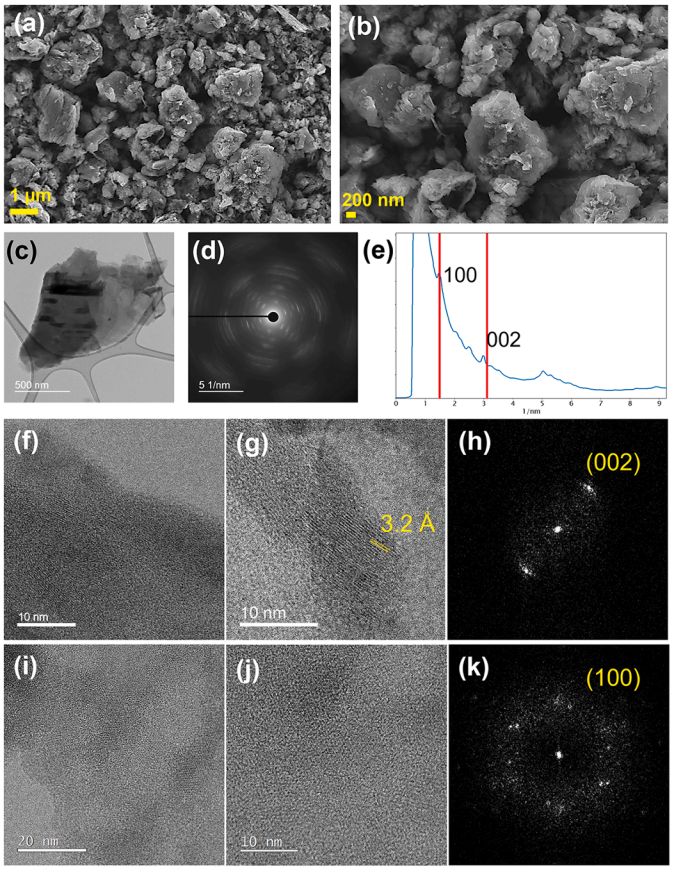

Fig. 2. Morphological and structural characterization of few-layer GCN by SEM and TEM analyses. (a, b) SEM images at different magnifications showing a few-layer GCN nanosheets stacked into a densely packed architecture. (c) TEM image revealing piled-up sheet-like flakes of GCN. (d) Corresponding SAED pattern showing texture and turbostratic-like characteristics in the microstructure. (e) Radial average profile with typical planes of GCN: (100) with d = 6.7 Å and (002) with 3.2 Å. High-resolution BF-STEM images of GCN (f, g) side-view and (i, j) top-view with the corresponding (h, k) fast Fourier transform (FFT) pattern confirming the triazine-based layered structure of GCN.

between bulk layered structures and a few-layered nanosheets. In contrast, the TEM images and AFM thickness measurements indicate thinner sheet-like structures, suggesting partial delamination of the layered material after the treatment process (Chouhan et al., 2023).

TEM analysis (Fig. 2c,d and e) further confirmed the presence of graphene-like nanosheets with flat morphology. The diffraction pattern revealed a textured structure with some indications of a turbostratic stacking (Fig. 2d). The diffraction streaks are better appreciated in the radial average profile in Fig. 2e, where the typical reference planes of GCN are labeled. Locally, the interplanar distances may vary in an asymmetric way, as seen also by other authors (Thomas et al., 2008). When the number of staking sheets increases, the characteristic planes become more evident, and the local features corresponding to a few stacking planes disappear (Figure S4), matching well with the XRD pattern from Fig. 1a, which represents a collective signal of the whole material. High-resolution STEM imaging was carried out to analyse the GCN layers closely. In Fig. 2f,g, a graphitic-like stacking arrangement in the material with an interlayer distance of 3.2 Å can be seen, which typically corresponds to 002 planes (Fig. 2h). A top view from a thin area is shown in Fig. 2i,j, where a few layers are stacked in a close to hexagonal arrangement, as evidenced by the fast Fourier transform in Fig. 2k. Apparent plane distances variations were observed between 6.0 and 6.7 Å in different areas. These variations have been argued to be potentially due to a tilted view and the creation of defects (Thomas et al., 2008).

To quantitatively evaluate nanosheet thickness, AFM measurements were performed over a calibrated scan area (~77–78 nm lateral dimensions), and the AFM images clearly show well-dispersed sheet-like domains with distinguishable height contrast relative to the substrate (Figure S5). The nanosheets are well dispersed on the substrate. Height profiles extracted from three independent cross-sectional lines reveal thicknesses in the range of approximately 1.5–1.8 nm relative to the substrate baseline. Considering the interlayer spacing of GCN (3.2 Å, consistent with the (002) XRD reflection), this thickness corresponds to approximately a few layers (2–4 stacked layers), confirming successful exfoliation into few-layer nanosheets rather than bulk stacked structure. Minor height variations observed in the profiles are attributed to surface roughness and tip sample convolution effects rather than intrinsic structural inhomogeneity.

The AFM-derived thickness values are in good agreement with the TEM images (Fig. 2c–k), which display highly transparent sheet-like morphologies and limited stacking. The combined SEM, TEM, SAED, and AFM analyses therefore provide complementary structural evidence confirming the successful synthesis of ultrathin, few-layered GCN nanosheets with preserved crystallinity and lamellar ordering. Such structural characteristics are critical for increasing surface accessibility and maximizing the availability of nitrogen coordination sites, thereby enhancing Hg^{2+} binding efficiency in DGT-based environmental applications.

The surface morphological and elemental distribution of the synthesized few-layer GCN nanosheets were further investigated using SEM coupled with energy-dispersive X-ray spectroscopy (EDS) (Figure S6). The SEM micrograph (Figure S6a) reveals the sheet-like morphology with relatively uniform surface features, consistent with the layered structure expected for exfoliated GCN. The absence of large, dense aggregates suggests effective delamination and good structural dispersion

of the nanosheets. Elemental mapping (Figures S6a,b) demonstrates a homogeneous spatial distribution of carbon and nitrogen across the nanosheets, confirming uniform incorporation of the primary framework elements. The corresponding EDS spectrum (Figure S6b) exhibits characteristic peaks attributable to carbon and nitrogen within the expected low-energy range (0.23–0.65 keV), consistent with the elemental composition of GCN. A minor oxygen signal is also detected, which is reasonably attributed to surface-adsorbed oxygen species, atmospheric exposure, or residual functional groups introduced during processing. Although EDS provides semi-quantitative information, the observed C/N ratio is consistent with the stoichiometric framework of GCN and supports the preservation of the nitrogen-rich heptazine structure. The slight oxygen contribution is typical for surface-modified or exfoliated carbon nitride materials.

These findings are in good agreement with complementary structural and chemical characterizations. XRD confirms the characteristic interlayer stacking and in-plane structural order of GCN, while FTIR identifies the typical vibrational bands associated with C–N and N–H bonding within the polymeric network. Furthermore, XPS analysis corroborates the elemental composition and chemical bonding states inferred from EDS, confirming the successful synthesis of structurally intact and compositionally homogeneous few-layer GCN nanosheets. These results provide consistent evidence for the formation of nitrogen-rich, layered GCN nanosheets with preserved structural integrity and uniform elemental distribution, which are essential for effective metal ion coordination and environmental applications.

3.3. Structural characterization of few-layer GCN via solid-state NMR spectroscopy

The structural integrity and chemical composition of the few-layer GCN nanosheets were analyzed using cross-polarization magic-angle spinning (CP-MAS) ^{13}C and ^{15}N solid-state NMR spectroscopy. This technique provided detailed information on the local chemical environments within polymeric GCN frameworks, particularly the triazine/heptazine units and their associated nitrogen coordination environments (Liu et al., 2016; Wang and Wang, 2022). Further investigation into the coordination of nitrogen species within the GCN structure was performed using ^{15}N and ^{13}C NMR spectra, which are shown in Figs. 3a and b.

The ^{15}N solid-state NMR spectrum exhibits four distinct resonance bands corresponding to different nitrogen environments in the GCN framework. The signal at –191 ppm is attributed to the outer nitrogen atoms, while the resonance at –226 ppm corresponds to the inner nitrogen species within the heptazine units (Fig. 3a). Two additional bands observed at –246 and –265 ppm are assigned to NH and NH_2 groups, respectively, originating from the terminal or partially condensed nitrogen species within the polymeric structure. These assignments are consistent with previously reported NMR studies of condensed GCN materials (Liu et al., 2016; Wang and Wang, 2022). The relatively weak intensity of the inner nitrogen signal at –226 ppm is attributed to its remote position from nearby protons, resulting in reduced dipolar coupling and lower cross-polarisation efficiency.

The ^{13}C CP-MAS NMR spectrum shows two prominent resonances at 155.44 and 164.45 ppm, which correspond to the inner and outer carbon atoms of the GCN framework (Fig. 3b). These signals arise from sp^2-hybridized carbon atoms in the N–C=N coordination environment within the triazine/heptazine units that form the polymeric graphitic carbon nitride network. The broader band centred around 164 ppm, with two discernible shoulders, indicates the presence of multiple carbon environments within the polymeric structure. Such variations likely originate from differences in local protonation states, partial deprotonation, or variations in the degree of polymerization of the GCN network.(Hu et al., 2017; Sehnert et al., 2007; Xu et al., 2016).

The observed spectral features confirm the presence of heptazine tectonic units forming the extended conjugated framework of graphitic carbon nitride, which governs the structural and electronic properties of the material. These NMR results are consistent with the structural information obtained from complementary characterization techniques, including XRD, FTIR, and XPS, which collectively confirm the formation of the layered graphitic carbon nitride framework (Binder et al., 2026).

Furthermore, similar spectral characteristics have been reported for GCN materials interacting with alkali metal salts such as KCl, where ion coordination occurs within the nitrogen-rich cavities of the heptazine framework (Gao et al., 2014). These findings demonstrate the robustness of the GCN structure and highlight the role of nitrogen coordination sites in governing ion interaction and adsorption behaviour.

3.4. Adsorption efficiency studies of GCN for Hg^{2+}

3.4.1. Effect of pH on Hg^{2+} adsorption

The adsorption behaviour of Hg^{2+} onto GCN was investigated over a pH range of 2–12 at a fixed Hg^{2+} concentration of 100 ng/mL (Fig. 4a). Adsorption efficiency strongly depends on the solution pH due to variations in surface charge and mercury speciation. Previous studies have reported that GCN typically exhibits a point of zero charge (pZC) in the range of approximately 5–7, depending on synthesis conditions and surface functional groups. This information is used here to qualitatively interpret the observed pH-dependent adsorption behavior (Chouhan et al., 2023). Maximum adsorption was observed at pH ≈ 7, where electrostatic attraction and coordination interactions between Hg^{2+} ions are favoured (Chouhan et al., 2023). These interactions promote the

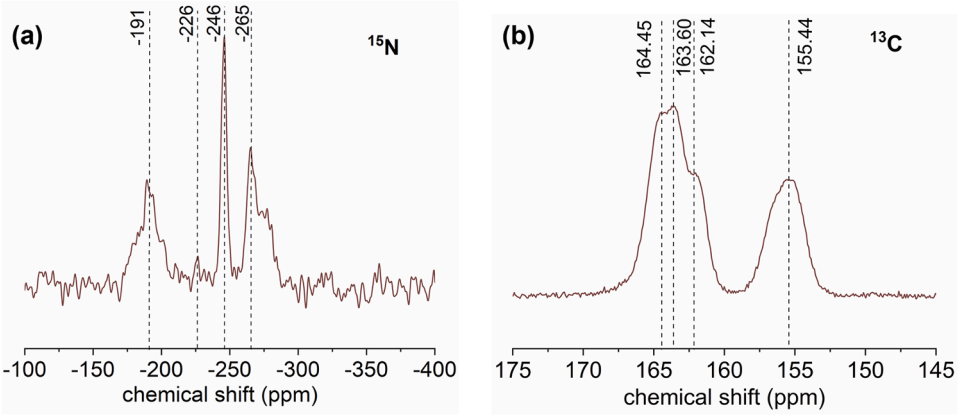

Fig. 3. Solid-state ^{15}N and ^{13}C CP-MAS NMR spectra of GCN. (a) ^{15}N spectrum shows four resonances at –191, –226, –246, and –265 ppm, assigned to outer/inner nitrogen atoms and NH/NH_2 groups, confirming a hydrogen-bonded melon-type structure. (b) ^{13}C spectrum exhibits peaks at 155 and 164 ppm corresponding to inner and outer carbon atoms of heptazine units, verifying the heptazine-based GCN framework and its local structural heterogeneity.

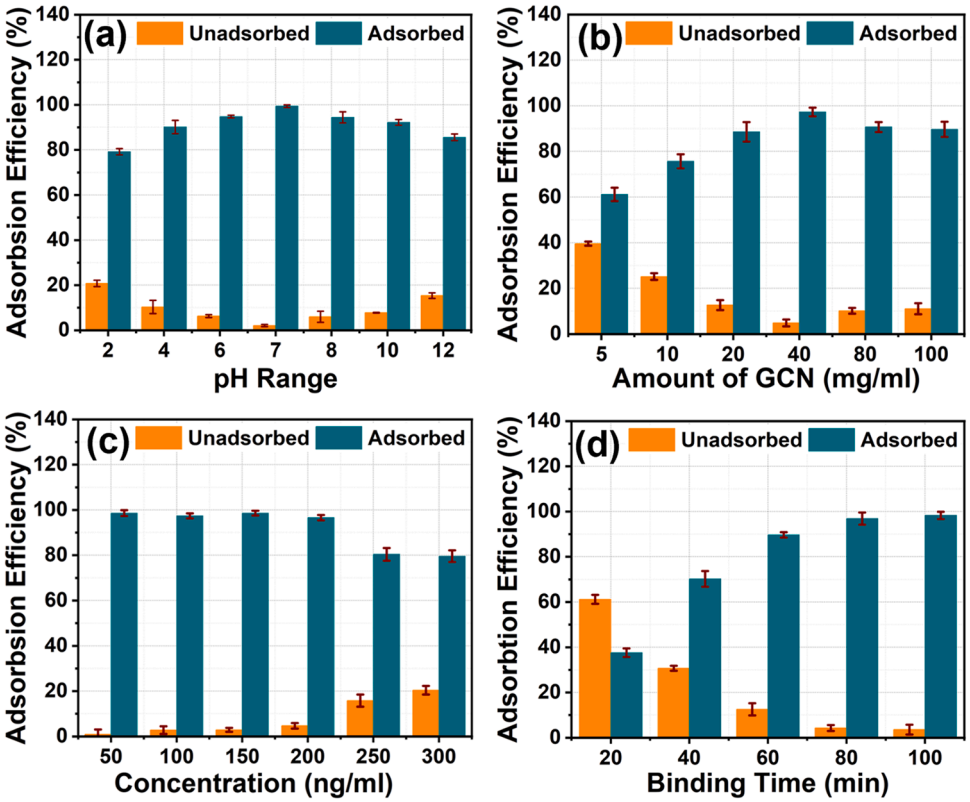

Fig. 4. Adsorption performance of GCN toward Hg^{2+} under different experimental conditions. (a) Effect of solution pH on Hg^{2+} adsorption. (b) Influence of GCN dosage on the adsorption efficiency for a Hg^{2+} concentration of 100 ng/mL. (c) Adsorption efficiency of GCN (40 mg/mL) at varying Hg^{2+} concentrations, and (d) Effect of contact time on Hg^{2+} adsorption under optimized conditions.

formation of stable Hg–N coordination complexes (Figure S7). In addition to surface charge effects, the adsorption behavior of Hg^{2+} is also influenced by the speciation of mercury in aqueous solution. Under acidic to near-neutral conditions, mercury predominantly exists as cationic species such as Hg^{2+} and $HgNO_3^+$, which can interact strongly with the electron-rich nitrogen sites of the GCN framework through coordination interactions. At higher pH values, hydrolysis reactions may occur, leading to the formation of species such as $Hg(OH)_2$, which can alter the adsorption behavior. Based on these observations, pH 7 was selected for subsequent adsorption experiments. It should be noted that the pZC value discussed here is based on literature reports for similar GCN materials rather than on a direct experimental measurement performed in this study.

3.4.2. *Influence of GCN dosage and mercury concentration*

The effect of GCN dosage was examined by varying the adsorbent concentration from 5 to 100 mg/mL at a constant Hg^{2+} concentration of 100 ng/mL (Fig. 4b). Adsorption efficiency increased with increasing GCN dosage due to the greater availability of active binding sites, reaching a maximum at 40 mg/mL. At higher dosages (80–100 mg/mL), a slight decline in efficiency was observed, likely due to aggregation or restacking of few-layer GCN nanosheets that reduces accessible surface area. Therefore, 40 mg/mL was selected as the optimal dosage. The influence of initial Hg^{2+} concentration was further evaluated over 50–300 ng/mL (Fig. 4c). Adsorption efficiency remained nearly constant (~95%) up to 200 ng/mL, but decreased to ~75% at 300 ng/mL, indicating progressive saturation of available coordination sites. These results demonstrate that GCN exhibits strong affinity toward Hg^{2+} at trace concentrations, although adsorption capacity becomes limited at higher concentrations.

3.4.3. *Effect of contact time*

Time-dependent adsorption experiments were conducted at an initial Hg^{2+} concentration of 100 ng/mL and the optimized GCN dosage (40 mg/mL) with contact times ranging from 20 to 100 min (Fig. 4d). During the initial 20 min, adsorption was relatively slow, leaving approximately 60% of Hg^{2+} in solution. As contact time increased to 60 min, adsorption efficiency increased significantly due to enhanced interaction between Hg^{2+} ions and nitrogen-containing functional groups on the GCN surface. At 80 min, the adsorption efficiency reached approximately 97%, and equilibrium was achieved within 100 min. The observed adsorption behaviour suggests a combined physisorption–chemisorption mechanism, where initial electrostatic attraction facilitates rapid diffusion of Hg^{2+} ions toward the GCN surface, followed by stronger coordination bonding between Hg^{2+} and nitrogen donor atoms within the heptazine structure. Such interactions have been widely reported for nitrogen-rich carbon nitride materials and contribute to the high affinity of GCN toward heavy metal ions. Notably, the synthesized GCN exhibited strong affinity and selectivity for Hg^{2+} at trace concentrations while requiring relatively low adsorbent dosage compared with other nanomaterial-based systems (Awual, 2017; Haseen et al., 2024).

3.5. *Performance evaluation of the GCN-Embedded binding layer for Hg^{2+} capture in DGT studies*

3.5.1. *Adsorption behavior under environmentally relevant conditions*

The adsorption performance of the AG–GCN composite gel was evaluated under environmentally relevant conditions using agarose gel (AG), AG–GCN composite gel, and bare GCN as control materials. Experiments were conducted for 24 h at near-neutral pH (6.5), simulating natural aquatic environments. As shown in Fig. 5a, bare GCN exhibited the highest adsorption capacity, binding 99% of Hg^{2+} (5 ng/mL). This high performance is attributed to the nitrogen-rich framework of GCN,

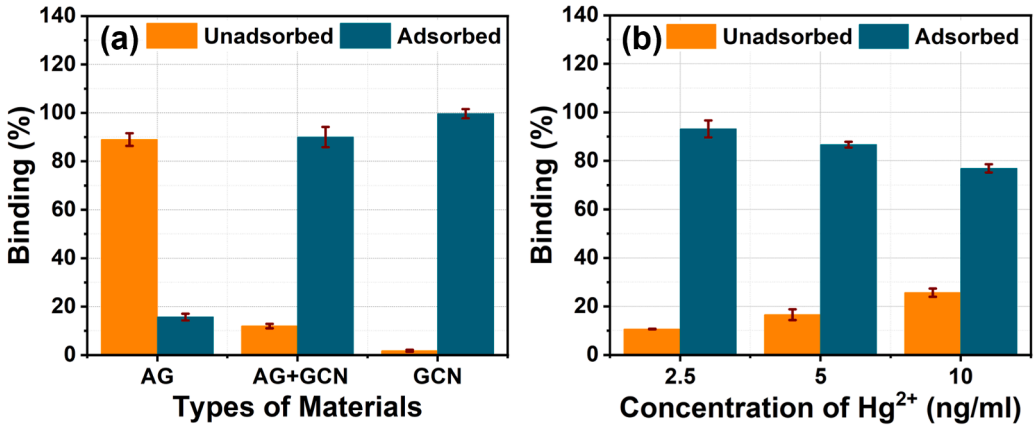

Fig. 5. Evaluation of Hg^{2+} binding performance of the gel matrices. (a) Adsorption efficiency of agarose gel (AG), AG–GCN composite gel, and bare GCN toward Hg^{2+} (5 ng/mL) after 24 h. (b) Concentration-dependent binding efficiency of the AG–GCN composite toward Hg^{2+} solutions.

where electron-donating functional groups such as amine and cyano moieties act as coordination sites for Hg^{2+} through Lewis acid–base interactions, forming stable Hg–N complexes.

The AG–GCN composite gel showed slightly lower adsorption efficiency (91.7%) due to partial encapsulation of GCN within the agarose matrix, which limits active-site accessibility and slows ion diffusion. In contrast, agarose gel alone exhibited minimal adsorption (13.7%), mainly governed by weak hydrogen bonding and nonspecific electrostatic interactions (Shorie et al., 2019). Overall, the adsorption trend followed GCN > AG–GCN > AG, confirming that GCN is the primary component responsible for Hg^{2+} capture.

3.5.2. *Concentration-dependent binding efficiency*

The influence of Hg^{2+} concentration on adsorption behaviour was examined over 2.5–10 ng /mL (Fig. 5b). The gels were exposed to Hg^{2+} solutions for 24 h under gentle agitation to simulate natural hydrodynamic conditions. At 2.5 ng/mL, AG–GCN discs bound approximately 93% of Hg^{2+}, leaving only trace residual mercury in solution. As the Hg^{2+} concentration increased to 5 and 10 ng/mL, the proportion of unbound ions increased, indicating a gradual decline in binding efficiency.

This behaviour is attributed to progressive saturation of active sites on the GCN surface combined with diffusion limitations within the agarose matrix. The relatively low GCN loading (4.92 mg per disc) limits the number of accessible adsorption sites relative to the Hg^{2+} concentration. Previous studies with bare GCN suspensions reported similar trends, where lower adsorbent loadings (5–10 mg/mL) showed reduced binding efficiency, whereas higher loadings (40 mg/mL) enabled near-complete adsorption equilibrium (Fig. 5b). Theoretical estimates indicate that 4.92 mg of GCN could bind up to ~10.72 mg of Hg^{2+}, suggesting that the observed decrease in efficiency is mainly governed by diffusion resistance rather than intrinsic adsorption capacity. The relatively low GCN loading (4.92 mg per disc) further restricts the total number of available binding sites within the composite gel. Additional evidence of diffusion limitations is provided by the kinetic comparison between AG–GCN and bare GCN systems, where adsorption equilibrium was reached within approximately 2 h for bare GCN but required 24 h for the AG–GCN composite due to slower Hg^{2+} transport through the agarose network. These observations collectively indicate that both active-site availability and diffusion resistance within the gel matrix influence the apparent adsorption efficiency of the composite.

To further evaluate the influence of coexisting ions on Hg^{2+} adsorption, interference experiments were performed in the presence of common ions typically found in natural water (river) systems. The experiments were carried out in solutions containing Hg^{2+} together with potential competing ions, including Na^{+}, K^{+}, Ca^{2+}, Ag^{+}, Co^{2+}, Zn^{2+}, Fe^{3+}, Mn^{2+}, Ni^{2+}, Bi^{3+}, Cl^{-}, Br^{-} and I^{-}. The adsorption behavior was assessed based on the percentage recovery of Hg^{2+} in the presence of these ions. As shown in Figure S8, the presence of these interfering species had only a limited effect on Hg^{2+} recovery. This behavior indicates that the adsorption process is largely governed by the strong interaction between Hg^{2+} ions and the nitrogen-rich active sites present in the GCN framework.

3.5.3. *Effect of mercury speciation on adsorption performance*

The influence of mercury speciation was evaluated using $HgCl_2$ as the mercury source (Figure S9). Both AG–GCN and bare GCN showed negligible adsorption (≤10%), indicating a strong dependence of adsorption on mercury speciation. In aqueous mercury nitrate systems, mercury mainly exists as cationic species such as Hg^{2+}, $HgNO_3^{+}$, and $Hg(NO_3)_2$ (Cotton et al., 1999). These ions readily coordinate with electron-rich nitrogen atoms in the GCN heptazine structure, forming stable Hg–N complexes through Lewis acid–base interactions. In contrast, $HgCl_2$ and chloro-complexes (e.g., $[HgCl_4]^{2-}$) are neutral or negatively charged species that interact weakly with the GCN surface, resulting in poor adsorption efficiency. These results demonstrate that GCN preferentially adsorbs cationic mercury species, highlighting the important role of mercury speciation in determining adsorption behaviour. Overall, embedding GCN within agarose produces a diffusion-regulated binding layer capable of selective Hg^{2+} uptake, making the AG–GCN composite a promising material for DGT-based in-situ mercury monitoring.

In the present study, structural characterization was mainly conducted on the few-layer GCN nanosheets, which constitute the active adsorption component of the AG–GCN composite. Techniques such as SEM, TEM, XRD, FTIR, NMR, and XPS confirmed the structural integrity of the synthesized GCN prior to its incorporation into the agarose matrix. Direct structural characterization of the AG–GCN composite is more challenging because the few-layer GCN nanosheets are embedded within the agarose gel network. In addition, since the AG–GCN gel is intended to function as a binding phase for DGT-based monitoring, it is generally designed for single-use deployment rather than repeated regeneration cycles. Therefore, the primary objective of this work was to evaluate the Hg^{2+} adsorption behaviour and binding performance of the system. Investigation of the long-term stability and potential reusability of AG–GCN composites will be addressed in future studies.

4. Conclusion

This study demonstrates, for the first time, the successful application of few-layer GCN nanosheets as a sustainable and metal-free binding material for mercury monitoring in DGT systems. Structural characterization by XRD, FTIR, XPS, TEM, AFM, and solid-state NMR confirmed

the formation of few-layer GCN nanosheets with a nitrogen-rich heptazine framework providing abundant coordination sites.

Batch adsorption experiments revealed strong Hg^{2+} affinity, with optimal performance at near-neutral pH and rapid adsorption kinetics reaching equilibrium within 100 min. The GCN nanosheets exhibited high adsorption efficiency (~97%) under optimized conditions, attributed to coordination interactions between Hg^{2+} ions and electron-donating nitrogen atoms. When incorporated into an agarose matrix, the AG–GCN composite binding layer demonstrated high mercury binding efficiency (>90%) at environmentally relevant concentrations (2.5–10 ng/mL), confirming its suitability for passive environmental monitoring applications. Compared with conventional DGT binding materials, the proposed GCN-based system offers several advantages, including metal-free composition, simple synthesis, chemical stability, and improved sustainability. The coordination-driven binding mechanism provides strong affinity toward mercury while maintaining compatibility with aqueous environmental matrices.

These findings establish GCN as a promising next-generation binding material for DGT devices. Future work will focus on evaluating long-term deployment stability, expanding selectivity studies in complex environmental waters, and extending this approach to other toxic metal ions. The integration of nitrogen-rich two-dimensional materials into passive sampling platforms opens new opportunities for sustainable and advanced environmental monitoring technologies.

Funding information

The Slovenian Research and Innovation Agency is acknowledged through funding the P1–0143 program and research projects J2–70096, J1–70019, N1–0100, L7–70280, N4–0351, J4–4556, BI-US/22–24–162, BI-LV/25–27–004, J1–3033, and J7–60123 projects. The authors also acknowledge the financial support of the European Commission (Grant Agreements No 826312, No 952379, No 101060211 and No 101183128).

CRediT authorship contribution statement

Dmitrii Deev: Writing – review & editing, Writing – original draft, Validation, Software, Methodology, Investigation, Formal analysis. **Raghuraj Singh Chouhan:** Writing – review & editing, Writing – original draft, Validation, Software, Project administration, Methodology, Investigation, Formal analysis, Conceptualization. **Igor Živković:** Writing – review & editing, Methodology, Investigation. **Ermira Begu:** Resources, Methodology, Investigation, Formal analysis. **Ana Drinčić:** Writing – review & editing, Resources, Methodology, Formal analysis. **Francisco Ruiz-Zepeda:** Writing – review & editing, Software, Formal analysis, Data curation. **Andraž Krajnc:** Writing – review & editing, Software, Formal analysis, Data curation. **Ivan Jerman:** Writing – review & editing, Validation, Software, Project administration, Methodology, Investigation, Formal analysis. **Roman Viter:** Writing – review & editing, Validation, Software, Formal analysis, Data curation. **Aleš Lapanje:** Writing – review & editing, Supervision, Project administration, Investigation, Funding acquisition. **Milena Horvat:** Writing – review & editing, Supervision, Project administration, Methodology, Funding acquisition, Conceptualization.

Declaration of competing interest

The authors declare that they have no known competing financial interests or personal relationships that could have appeared to influence the work reported in this paper.

Acknowledgements

The Slovenian Research and Innovation Agency is acknowledged through funding the P1-0143 program and research projects J2-70096, J1-70019, N1-0100, L7-70280, N4-0351, J4-4556, BI-US/22–24–162, BI-LV/25–27–004, J1-3033, and J7-60123 projects. The authors also acknowledge the financial support of the European Commission (Grant Agreements No 826312, No 952379, No 101060211 and No 101183128).

Supplementary materials

Supplementary material associated with this article can be found, in the online version, at doi:10.1016/j.hazadv.2026.101190.

Data availability

Data will be made available on request.

References

Alizadeh, T., Nayeri, S., Hamidi, N., 2019. Graphitic carbon nitride (g-C 3 N 4)/graphite nanocomposite as an extraordinarily sensitive sensor for sub-micromolar detection of oxalic acid in biological samples. RSC Adv. 9, 13096–13103. https://doi.org/10.1039/C9RA00982E.

Amouzadeh Tabrizi, M., Nazari, L., Acedo, P., 2021. A photo-electrochemical aptasensor for the determination of severe acute respiratory syndrome coronavirus 2 receptor-binding domain by using graphitic carbon nitride-cadmium sulfide quantum dots nanocomposite. Sensors Actuators B Chem. 345, 130377. https://doi.org/10.1016/j.snb.2021.130377.

Awual, M.R., 2017. Novel nanocomposite materials for efficient and selective mercury ions capturing from wastewater. Chem. Eng. J. https://doi.org/10.1016/j.cej.2016.08.108.

Benedet, M., Andrea Rizzi, G., Gasparotto, A., Gauquelin, N., Orekhov, A., Verbeeck, J., Maccato, C., Barreca, D., 2023. Functionalization of graphitic carbon nitride systems by cobalt and cobalt-iron oxides boosts solar water oxidation performances. Appl. Surf. Sci. 618, 156652. https://doi.org/10.1016/j.apsusc.2023.156652.

Benedet, M., Andrea Rizzi, G., Gasparotto, A., Lebedev, O.I., Girardi, L., Maccato, C., Barreca, D., 2022a. Tailoring oxygen evolution performances of carbon nitride systems fabricated by electrophoresis through Ag and Au plasma functionalization. Chem. Eng. J. 448, 137645. https://doi.org/10.1016/j.cej.2022.137645.

Benedet, M., Gasparotto, A., Rizzi, G.A., Barreca, D., Maccato, C., 2022b. g-C3N4-based materials functionalized with Au, Ag, and Au-Ag: an XPS study. Surf. Sci. Spectra 29. https://doi.org/10.1116/6.0002028.

Binder, F., Moudrakovski, I., Kötter, N.L., Das, S., Küster, K., Bette, S., Lotsch, B.V., 2026. Covalent surface functionalization of carbon nitrides: a case study of poly(heptazine imide). Mater. Adv. 7, 1814–1824. https://doi.org/10.1039/D5MA01345C.

Botelho, C.N., Falcão, S.S., Soares, R.-E.P., Pereira, S.R., de Menezes, A.S., Kubota, L.T., Damos, F.S., Luz, R.C.S., 2022. Evaluation of a photoelectrochemical platform based on strontium titanate, sulfur doped carbon nitride and palladium nanoparticles for detection of SARS-CoV-2 spike glycoprotein S1. Biosens. Bioelectron. X 11, 100167. https://doi.org/10.1016/j.biosx.2022.100167.

Chouhan, R.S., Gačnik, J., Živković, I., Vijayakumaran Nair, S., Van de Velde, N., Vesel, A., Šket, P., Gandhi, S., Jerman, I., Horvat, M., 2023. Green synthesis of a magnetite/graphitic carbon nitride 2D nanocomposite for efficient Hg 2+ remediation. Environ. Sci. Nano 10, 2658–2671. https://doi.org/10.1039/D3EN00367A.

Chouhan, R.S., Jerman, I., Heath, D., Bohm, S., Gandhi, S., Sadhu, V., Baker, S., Horvat, M., 2021. Emerging tri-s-triazine-based graphitic carbon nitride: a potential signal-transducing nanostructured material for sensor applications. Nano Sel. 2, 712–743. https://doi.org/10.1002/nano.202000228.

Chouhan, R.S., Žitko, G., Fajon, V., Živković, I., Pavlin, M., Berisha, S., Jerman, I., Vesel, A., Horvat, M., 2019. A unique interactive nanostructure knitting based passive sampler adsorbent for monitoring of Hg2+ in water. Sensors 19, 3432. https://doi.org/10.3390/s19153432.

Cotton, F.A., Wilkinson, G., Murillo, C.a., Bochmann, M., 1999. Advanced Inorganic Chemistry, 6th Edition. Wiley-Interscience, New York.

Dyjak, S., Kiciński, W., Huczko, A., 2015. Thermite-driven melamine condensation to C x N y H z graphitic ternary polymers: towards an instant, large-scale synthesis of g-C 3 N 4. J. Mater. Chem. A 3, 9621–9631. https://doi.org/10.1039/C5TA00201J.

Eckley, C.S., Eagles-Smith, C., Luxton, T.P., Hoffman, J., Janssen, S., 2023. Using mercury stable isotope fractionation to identify the contribution of historical mercury mining sources present in downstream water, sediment and fish. Front. Environ. Chem. 4. https://doi.org/10.3389/fenvc.2023.1096199.

Elias, G., Díez, S., Zhang, H., Fontàs, C., 2020. Development of a new binding phase for the diffusive gradients in thin films technique based on an ionic liquid for mercury determination. Chemosphere 245, 125671. https://doi.org/10.1016/j.chemosphere.2019.125671.

Gade, C., Mbadugha, L., Paton, G., 2024. Use of diffusive gradient in thin-films (DGTs) to advance environmental mercury research: development, growth, and tomorrow. Trends Environ. Anal. Chem. 42, e00230. https://doi.org/10.1016/j.teac.2024.e00230.

Gao, H., Yan, S., Wang, J., Zou, Z., 2014. Ion coordination significantly enhances the photocatalytic activity of graphitic-phase carbon nitride. Dalt. Trans. 43, 8178–8183. https://doi.org/10.1039/C3DT53224K.

Haseen, U., Ali, S.G., Khan, R.A., Alsalme, A., Koo, B.H., Ahmad, H., 2024. Preconcentration and selective extraction of trace Hg(<scp>ii</scp>) by polymeric g-C $_3$ N $_4$ nanosheet-packed SPE column. RSC Adv. 14, 1593–1601. https://doi.org/10.1039/D3RA05512D.

Hasija, V., Patial, S., Singh, P., Nguyen, V.-H., Le, Q.Van, Thakur, V.K., Hussain, C.M., Selvasembian, R., Huang, C.-W., Thakur, S., Raizada, P., 2021. Photocatalytic inactivation of viruses using graphitic carbon nitride-based photocatalysts: virucidal performance and mechanism. Catalysts 11, 1448. https://doi.org/10.3390/catal11121448.

Hu, Y., Shim, Y., Oh, J., Park, Sunghee, Park, Sungjin, Ishii, Y., 2017. Synthesis of 13 C-, 15 N-labeled graphitic carbon nitrides and NMR-based evidence of hydrogen-bonding assisted two-dimensional assembly. Chem. Mater. 29, 5080–5089. https://doi.org/10.1021/acs.chemmater.7b00069.

Idris, A.O., Oseghe, E.O., Msagati, T.A.M., Kuvarega, A.T., Feleni, U., Mamba, B., 2020. Graphitic carbon nitride: a highly electroactive nanomaterial for environmental and clinical sensing. Sensors 20, 5743. https://doi.org/10.3390/s20205743.

Kreuzeder, A., Santner, J., Zhang, H., Prohaska, T., Wenzel, W.W., 2015. Uncertainty evaluation of the diffusive gradients in thin films technique. Environ. Sci. Technol. 49, 1594–1602. https://doi.org/10.1021/es504533e.

Liao, Q., Pan, W., Zou, D., Shen, R., Sheng, G., Li, X., Zhu, Y., Dong, L., Asiri, A.M., Alamry, K.A., Linghu, W., 2018. Using of g-C 3 N 4 nanosheets for the highly efficient scavenging of heavy metals at environmental relevant concentrations. J. Mol. Liq. 261, 32–40. https://doi.org/10.1016/j.molliq.2018.03.093.

Lin, H., Li, Mingzhi, Zhu, Y., Lan, W., Feng, Q., Ding, S., Li, T., Wang, Y., Duan, Y., Wei, J., Li, Mingen, 2022. Development and validation of the DGT technique using the novel cryogel for measuring dissolved Hg(II) in the estuary. Mar. Environ. Res. 182, 105773. https://doi.org/10.1016/j.marenvres.2022.105773.

Liu, J., Wang, H., Antonietti, M., 2016. Graphitic carbon nitride “reloaded”: emerging applications beyond (photo)catalysis. Chem. Soc. Rev. 45, 2308–2326. https://doi.org/10.1039/C5CS00767D.

Lv, J., Wu, X., Lin, H., Feng, Q., Lan, W., Li, M., Chen, Z., Li, L., Ding, S., Wang, Y., Wei, J., Duan, Y., He, J., 2025. The MoS2/rGO embed in macro-porous PAN gel as a novel DGT binding phase for the rapid and accurate detection of trace Hg(II). Talanta 283, 127124. https://doi.org/10.1016/j.talanta.2024.127124.

Marchiori, G., Seraglia, R., Rizzi, G.A., Maccato, C., Benedet, M., Callone, E., Dirè, S., Gasparotto, A., Barreca, D., 2025. Defect-engineered graphitic carbon nitride on carbon cloth supports for the photoelectrocatalytic degradation of organophosphate pesticides. RSC Appl. Interfaces 2, 104–113. https://doi.org/10.1039/D4LF00259H.

Marrugo-Madrid, S., Marrugo-Negrete, J., Queralt, I., Palet, C., Díez, S., 2024. Evaluation of novel biomass-derived materials as binding layers for determining labile mercury in water by diffusive gradient in thin-films technique. Talanta 267, 125227. https://doi.org/10.1016/j.talanta.2023.125227.

Mason, R.P., Choi, A.L., Fitzgerald, W.F., Hammerschmidt, C.R., Lamborg, C.H., Soerensen, A.L., Sunderland, E.M., 2012. Mercury biogeochemical cycling in the ocean and policy implications. Environ. Res. 119, 101–117. https://doi.org/10.1016/j.envres.2012.03.013.

Noh, S., Kim, Y., Kim, H., Seok, K., Park, M., Bailon, M.X., Hong, Y., 2020. The performance of diffusive gradient in thin film probes for the long-term monitoring of trace level total mercury in water. Environ. Monit. Assess. 192, 66. https://doi.org/10.1007/s10661-019-7966-2.

Pelcová, P., Ridošková, A., Hrachovinová, J., Grmela, J., 2021. Evaluation of mercury bioavailability to vegetables in the vicinity of cinnabar mine. Environ. Pollut. 283, 117092. https://doi.org/10.1016/j.envpol.2021.117092.

Pi, K., Liu, J., Van Cappellen, P., 2020. Direct measurement of aqueous mercury(II): combining DNA-based sensing with diffusive gradients in thin films. Environ. Sci. Technol. 54, 13680–13689. https://doi.org/10.1021/acs.est.0c03870.

Reichstädter, M., Gao, Y., Diviš, P., Ma, T., Gaulier, C., Leermakers, M., 2021. Cysteine-modified silica resin in DGT samplers for mercury and trace metals assessment. Chemosphere 263, 128320. https://doi.org/10.1016/j.chemosphere.2020.128320.

Rodríguez Martín-Doimeadios, R.C., Monperrus, M., Krupp, E., Amouroux, D., Donard, O.F.X., 2003. Using speciated isotope dilution with GC−inductively coupled plasma MS to determine and unravel the artificial formation of monomethylmercury in certified reference sediments. Anal. Chem. 75, 3202–3211. https://doi.org/10.1021/ac026411a.

Rodríguez Martín-Doimeadios, R.C., Tessier, E., Amouroux, D., Guyoneaud, R., Duran, R., Caumette, P., Donard, O.F.X., 2004. Mercury methylation/demethylation and volatilization pathways in estuarine sediment slurries using species-specific enriched stable isotopes. Mar. Chem. 90, 107–123. https://doi.org/10.1016/j.marchem.2004.02.022.

Sehnert, J., Baerwinkel, K., Senker, J., 2007. Ab initio calculation of solid-State NMR spectra for different triazine and heptazine based structure proposals of g-C 3 N 4. J. Phys. Chem. B 111, 10671–10680. https://doi.org/10.1021/jp072001k.

Shorie, M., Kaur, H., Chadha, G., Singh, K., Sabherwal, P., 2019. Graphitic carbon nitride QDs impregnated biocompatible agarose cartridge for removal of heavy metals from contaminated water samples. J. Hazard. Mater. 367, 629–638. https://doi.org/10.1016/j.jhazmat.2018.12.115.

Song, S., Li, Y., Liu, Q.S., Wang, H., Li, P., Shi, J., Hu, L., Zhang, H., Liu, Y., Li, K., Zhao, X., Cai, Z., 2021. Interaction of mercury ion (Hg2+) with blood and cytotoxicity attenuation by serum albumin binding. J. Hazard. Mater. 412, 125158. https://doi.org/10.1016/j.jhazmat.2021.125158.

Sreenivasulu, M., Malode, S.J., Alodhayb, A.N., Shetti, N.P., 2024. Exfoliated 2-D graphitic carbon nitride nanosheets for electrochemical detection of the antiviral drug Valganciclovir. Electrocatalysis 15, 456–473. https://doi.org/10.1007/s12678-024-00887-6.

Sun, S., Gou, X., Tao, S., Cui, J., Li, J., Yang, Q., Liang, S., Yang, Z., 2019. Mesoporous graphitic carbon nitride (g-C 3 N 4) nanosheets synthesized from carbonated beverage-reformed commercial melamine for enhanced photocatalytic hydrogen evolution. Mater. Chem. Front. 3, 597–605. https://doi.org/10.1039/C8QM00577J.

Thomas, A., Fischer, A., Goettmann, F., Antonietti, M., Müller, J.-O., Schlögl, R., Carlsson, J.M., 2008. Graphitic carbon nitride materials: variation of structure and morphology and their use as metal-free catalysts. J. Mater. Chem. 18, 4893. https://doi.org/10.1039/b800274f.

UNEP, 2018. Technical Background Report to the Global Mercury Assessment 2018. UNEP.

Wang, J., Wang, S., 2022. A critical review on graphitic carbon nitride (g-C3N4)-based materials: preparation, modification and environmental application. Coord. Chem. Rev. https://doi.org/10.1016/j.ccr.2021.214338.

Xu, J., Shang, J.-K., Jiang, Q., Wang, Y., Li, Y.-X., 2016. Facile alkali-assisted synthesis of g-C 3 N 4 materials and their high-performance catalytic application in solvent-free cycloaddition of CO 2 to epoxides. RSC Adv 6, 55382–55392. https://doi.org/10.1039/C6RA10509B.

Xu, Y., Gong, Y., Ren, H., Liu, W., Niu, L., Li, C., Liu, X., 2017. In situ structural modification of graphitic carbon nitride by alkali halides and influence on photocatalytic activity. RSC Adv. 7, 32592–32600. https://doi.org/10.1039/C7RA05555B.

Yao, H., Zhao, Y., Lin, C.-J., Yi, F., Liang, X., Feng, X., 2020. Development of a novel composite resin for dissolved divalent mercury measurement using diffusive gradients in thin films. Chemosphere 251, 126231. https://doi.org/10.1016/j.chemosphere.2020.126231.

Yin, H., Yao, H., Yuan, W., Lin, C.-J., Fu, X., Yin, R., Meng, B., Luo, J., Feng, X., 2023. Determination of the isotopic composition of aqueous mercury in a paddy ecosystem using diffusive gradients in thin films. Anal. Chem. 95, 12290–12297. https://doi.org/10.1021/acs.analchem.3c01356.

Yu, Y., Zhou, Q., Wang, J., 2016. The ultra-rapid synthesis of 2D graphitic carbon nitride nanosheets via direct microwave heating for field emission. Chem. Commun. 52, 3396–3399. https://doi.org/10.1039/C5CC10258H.

Zhou, C., van de Velde, S., Baeyens, W., Gao, Y., 2018. Comparison of Chelex based resins in diffusive gradients in thin-film for high resolution assessment of metals. Talanta 186, 397–405. https://doi.org/10.1016/j.talanta.2018.04.085.